Effects of characteristic length scales on the exciton dynamics in rubrene single crystals

Björn Gieseking,[1] Teresa Schmeiler,[1] Benjamin Müller,[1] Carsten Deibel,[1] Bernd Engels,[2]
Vladimir Dyakonov,[1,3] and Jens Pflaum[1,3]

[1]*Experimental Physics VI, Julius-Maximillian University, D-97074 Würzburg, Germany*
[2]*Institute for Physical and Theoretical Chemistry, Julius-Maximillian University, D-97074 Würzburg, Germany*
[3]*Bavarian Center for Applied Energy Research e.V. (ZAE Bayern), D-97074 Würzburg, Germany*

We present temperature dependent time-resolved photoluminescence (PL) investigations on well-defined morphologies of the prototypical organic semiconductor rubrene. By their respective degree of spatial constraint these morphologies directly influence the temperature dependent excitonic processes and their dynamics. While in bulk single crystals singlet exciton decay is governed by thermally activated fission at a time constant of 20 ps, this mechanism appears to be absent in rubrene microcrystals. Here the dynamics are characterized by a pronounced increase of the average exciton lifetime as confirmed by the dominating PL decay channel with an effective time constant of 100 ps. The enhanced surface-to-volume ratio indicates that the participating states might originate from microcrystal boundaries which could be reached by the substantial amount of migrating excitons prior to the onset of other decay processes. The suppression of singlet fission in these crystalline microstructures is promoted by the significantly lower activation energy of 25 meV for the 100 ps channel compared to the singlet fission barrier of 44 meV and imposes severe consequences for its utilization in, e.g., thin film photovoltaics. For the crystalline samples, an additional relaxation channel with a time constant of around 500 ps becomes relevant at very low temperatures. As this process is the only one observed for amorphous rubrene thin films it points at the local nature of the underlying decay mechanism.

The transport of optically excited states, also referred to as excitons, defines a critical step in the light-to-charge carrier conversion in organic materials [1]. To overcome limitations by the short diffusion lengths of singlet excitons, the harvesting of triplet excitons generated via singlet fission has been suggested a possible approach to increase the conversion efficiency in organic photovoltaic cells [2,3]. Furthermore, upon miniaturization of up-to-date organic electronic devices the correlation between exciton transport and morphological length scales becomes increasingly important as the structural coherence significantly affects the photophysical processes and their time evolution [1,4,5]. Here we demonstrate the influence of spatial confinement on the excitonic states and their dynamics in the prototypical organic semiconductor rubrene. By its unique property of providing morphologies with different characteristic length scales we observe the direct structural influence on the temperature dependent photoluminescence (PL) spectra and on the relaxation processes within 10^{-12} s time scales already for excitation volumes with micrometer lateral extensions. Our results highlight the role of the local environment on the exciton dynamics in molecular semiconductors which has to be considered upon tailoring the microscopic morphology of organic optoelectronic devices.

Besides its remarkable photophysical behavior, characterized, e.g., by singlet fission in combination with extended lifetimes (μs) and diffusion lengths (μm) for the generated triplets [6–9], rubrene offers the possibility of different, well-controllable structural morphologies in combination with sufficiently high PL quantum yields. In thin films without further surfactants rubrene grows x-ray amorphous [10] due to an activation barrier of 210 meV [11] required for planarization of its conjugated backbone. In contrast, single crystals grown by vapor sublimation under streaming carrier gas show an exceptional structural quality characterized by micrometer-

sized crystalline facets as well as lateral extensions of several millimeters [12]. Adjusting the conditions during growth allows for a broad morphological variety of microstructures in-between, ranging from spatially defined microcrystals to self-organized pyramidal surface structures [13], all of which imposing different boundary conditions for photogenerated excitons and thus yielding to modifications of the optical characteristics.

For instance, a recent study on the directionality of the steady state absorption and emission suggests that variations of the PL spectra detected on rubrene microstructures originate from the anisotropic nature of emission [14]. Though the relative intensities can be explained by this approach it is insufficient to account for the temperature dependent optical phenomena and their temporal evolution on short time scales reported in this work.

Rubrene powder was purchased from Sigma Aldrich and further purified by gradient sublimation. Single crystals were grown afterwards by horizontal physical vapor transport (PVT) [15] in a constant stream of high-purity 6N nitrogen gas. The source temperature during growth was set to 280 °C and nucleation took place at a distance of approximately 10 cm from the source. Needle- and plateletlike crystals were obtained with lateral dimensions of several millimeters and thicknesses in the range of 100–300 μm. The achieved surfaces of the plateletlike crystals correspond to the (001)-rubrene crystal plane. Amorphous rubrene films of 30 nm thickness on sapphire substrates were grown by evaporation under high vacuum conditions at a rate of 0.5 nm/s. During deposition the layer thickness was monitored with an oscillating quartz crystal and afterwards confirmed by x-ray reflectivity measurements. For the microcrystals, rubrene powder was dissolved in tetrahydrofuran (THF) at a concentration of 1 mg/ml [16]. The solution was stirred for 10 min and then rapidly mixed with

distilled water. Upon this process microparticles were formed instantaneously. After stirring and ultrasonicating the solution for 10 min, amounts of several microliters were deposited on a glass substrate and kept drying at RT. Finally, by heating the substrate for several hours at a constant temperature of 180 °C microcrystals start forming.

X-ray diffraction (XRD) measurements of bulk single crystal and amorphous film were carried out in Bragg-Brentano geometry by means of a diffractometer model XRD 3003 T/T (GE Inspection Technologies) using $Cu-K\alpha$ radiation at a wavelength of 1.54 Å. Due to the low particle density, characterization of the precipitated microcrystals was performed by a scanning electron microscope SEM Ultra-Plus (Zeiss) using beam energies between 2 and 20 keV. To analyze the absorption properties of the single crystals, spectra were recorded by means of a Lambda 950 UV/VIS spectrometer (Perkin Elmer). The amorphous film was measured with a V630 UV-VIS spectrophotometer (Jasco). As the samples absorb in the visible, investigations were restricted to a wavelength range of 300–800 nm (4.13–1.55 eV). Transmission electron microscopy (TEM) studies on the microcrystals were carried out with a $FEI-Titan^{TM}$ TEM with beam energies of 300 keV. For this purpose, the microcrystals were deposited and thermally post-treated on a TEM copper grid. Finally, to carry out time-resolved PL measurements, the output of a Ti:Sa oscillator (Spectra Physics, 100 fs, 800 nm) was frequency doubled and focused onto the sample, which was mounted inside a liquid helium cryostat. By this arrangement, all samples were kept under vacuum during PL studies thus minimizing possible degradation via photo-oxidation at the surface. The fluence used for all time-resolved experiments was kept constant at $2.6\,nJ/cm^2$ and the polarization of the incident light was chosen parallel to the b direction in case of the rubrene single crystal measurements and arbitrary in case of the amorphous thin films and microcrystal ensembles. The PL signal was spectrally dispersed by a spectrograph and detected with a C 5680 streak camera (Hamamatsu). The temporal resolution of the setup employed was 8 ps and the maximum detection window was limited to 2 ns.

Following pulsed laser excitation we probed the temperature dependence of photoluminescence decay dynamics of the three types of rubrene morphologies with different structural hierarchies—bulk crystals, microcrystals, and amorphous thin films [Fig. 1(a)]. While the single crystals exhibit a high degree of crystallinity and domains exceeding several micrometers in length, the amorphous character of the thin films is deduced from the absence of Bragg peaks in the corresponding x-ray diffraction spectra (Fig. 4 in the Supplemental Material [17]). The crystallinity of the microstructures is indicated by the diffraction pattern derived from transmission electron microscopy as shown in Fig. 5 in the Supplemental Material [17]. By variation of their inherent length scales the different morphologies exhibit an increasing degree of spatial confinement for photogenerated excitons, which directly affects the time-integrated PL spectra (Fig. 1(b) and Fig. 6 in the Supplemental Material [17]), the latter being derived from the corresponding time-resolved data. Compared to the bulk spectrum, the high-energy peak (2.16 eV) is significantly enhanced in the microcrystal PL spectrum. This peak has been associated either with a charge transfer state [6] or a coherent excitonic state [13,18,19], whereas the lower energetic peaks (2.02, 1.88, and 1.74 eV) are attributed to emission from a localized molecular excitonic species with a vibronic progression of 140 meV [20,21]. However, since in our studies we observe a similar temperature dependent intensity behavior for all four peaks—a different temperature dependent behavior reported in literature might be due to variations in crystal quality caused, e.g., by oxygen-induced trap states during crystal growth [22]—and as their PL decay dynamics appear to be independent of the applied excitation power [Fig. 3(b)] we find no indication for the coexistence of two independent emitting species in rubrene. Therefore, we consider the radiative decay originating from just one singlet excitonic state with different polarizations to be the only contribution to the detected PL signal. The enhancement of the 2.16 eV peak in the spectra of the microcrystals can therefore be related to an enhanced emission polarized parallel to the c direction (M polarization) which can be detected from the side facets of the samples due to their small lateral
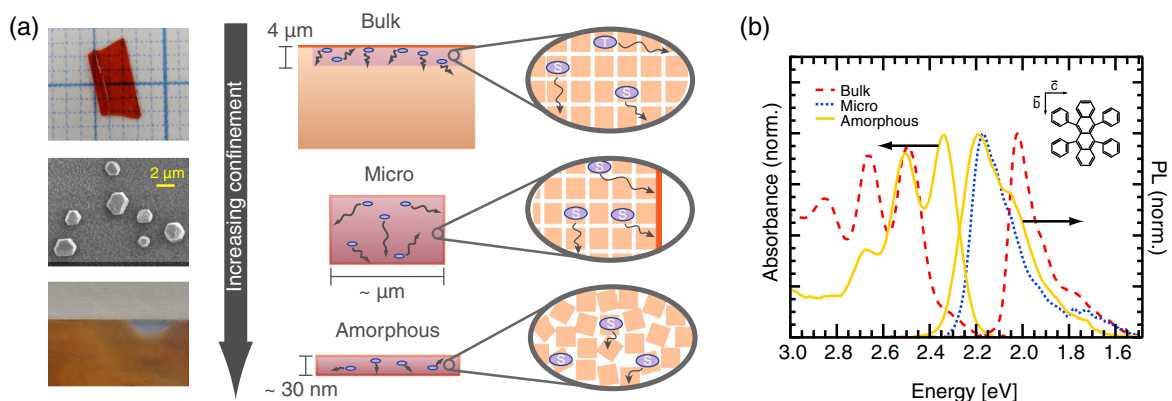

FIG. 1. (Color online) (a) Pictures of different samples and related morphologies of the excitation volumes schematically illustrating the effect of spatial confinement and different length scales on the created excitons. (b) Time-integrated PL spectra of rubrene bulk and microcrystals as well as of a thin amorphous film together with bulk crystal and amorphous film absorption (all spectra are normalized). The inset shows the molecular structure of rubrene together with the crystallographic directions of its unit cell.

extension in combination with a reduced self-absorption within the micrometer-sized crystalline volume [14].

The shape of the microcrystal PL is very similar to that of the amorphous layer, which can be explained by the fact that the directionality of emission and the enhanced out-coupling at the crystal edges resemble the random molecular orientation in the film [14]. However, the peak width of the latter is broadened due to the enhanced energetic disorder. As a result of this disorder, excitations—i.e., singlet excitons—are preferentially localized on molecular length scales and, in analogy to free charge carriers, are expected to exhibit a reduced mobility compared to crystalline samples [23]. Furthermore, by the neat hydrocarbon nature of rubrene the triplet quantum yield by intersystem crossing and thus effects on the population according to this relaxation channel are assumed to be negligible in accordance to observations on rubrene in solution [24,25].

Optical excitation of the two crystalline structures (bulk and microcrystal), in contrast, leads to creation of more mobile singlet excitons. At 4 K a lower limit for the exciton diffusion constant of $0.2\,\mathrm{cm^2/s}$ has been deduced from μ-PL measurements which is in line with values of more than $1\,\mathrm{cm^2/s}$ determined for other polyaromatic single crystals by transient grating experiments at cryogenic temperatures [13,26]. Therefore, providing long-range molecular ordering, singlet excitons are able to travel large distances before relaxing via radiative or nonradiative processes such as singlet fission [7] or quenching at defects or interfaces [27]. As a consequence, in spatially confined crystalline microstructures low-energy trapping sites induced by local disorder at the boundaries impose a significant influence on the decay dynamics, if reached by excitons [28]. We point out that owing to the faster growth kinetics during precipitation rubrene microcrystals might exhibit slightly smaller subdomains compared to sublimation grown bulk crystals and therefore, singlet excitons generated at the center of the microcrystals, i.e., far away from the outer boundaries, might experience trap-assisted relaxation at shorter migration lengths.

For the quantitative evaluation of the spectroscopic data it has to be considered that the PL intensity of the respective rubrene morphology at a given temperature corresponds to the area enclosed by the associated time-integrated PL spectrum. The analysis of the temperature dependence was carried out by assuming a radiative decay channel of rate γ_r together with a dominating thermally activated nonradiative relaxation of rate γ_{nr}:

$$\gamma = 1/\tau = \gamma_r + \gamma_{nr}e^{-\Delta E/kT}, \qquad (1)$$

with ΔE describing the activation energy of this channel. By this approach the photoluminescence efficiency can be expressed as $\eta = \gamma_r/\gamma$ [29] and was employed to fit the temperature dependent PL and thus to deduce the energy of the dominating decay channel for each sample. In order to correctly describe the low temperature behavior of the amorphous film the efficiency of singlet exciton generation was adapted by a temperature dependent prefactor in Eq. (1).

Appraising this microscopic model by temperature dependent PL studies on the various samples, the amorphous rubrene film initially shows a PL increase upon cooling from room temperature followed by a continuous drop of intensity

below 150 K [see Figs. 2(a) and 2(b)]. The primary rise of the PL signal with decreasing temperature can be ascribed to a suppression of thermally activated, nonradiative decay processes. The deduced barrier of $\Delta E_3 = 134$ meV is of the order of molecular vibrational energies and thus points at the local character of this decay channel. Below 150 K the lack of thermal energy promotes additional nonradiative decay channels, e.g., by static impurity quenching.

In contrast, cooling down the two crystalline sample morphologies to 8 K leads to a pronounced monotonous increase of the detected PL intensity [see Figs. 2(a) and 2(b)]. In accordance to the temperature dependent PL behavior of the amorphous film, the absolute change can be explained by the existence of a thermally activated nonradiative decay mechanism. For bulk and microcrystals, however, we deduce different barrier heights of $\Delta E_1 = 44$ and $\Delta E_2 = 25$ meV, respectively (see also Table I). These values are in agreement

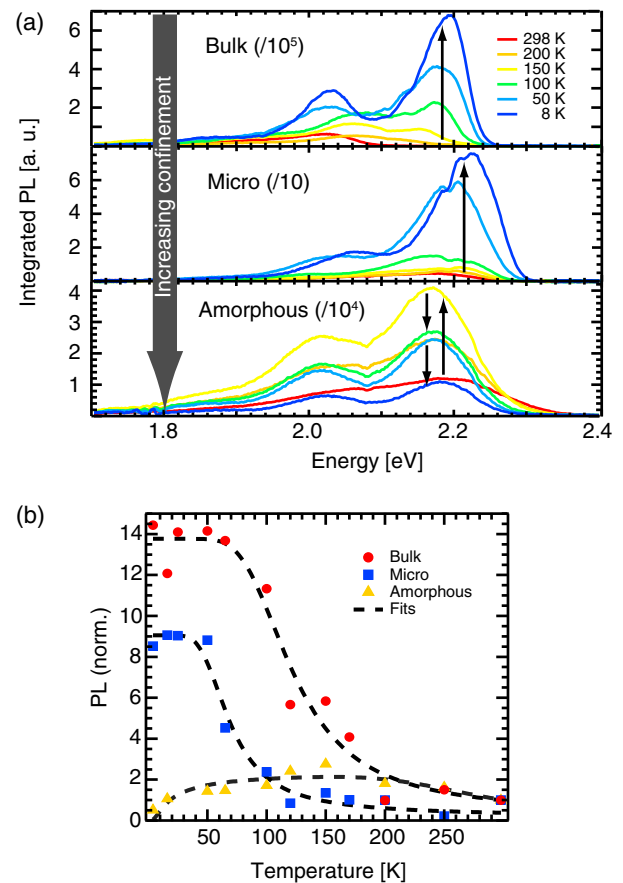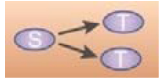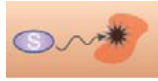FIG. 2. (Color online) (a) Integrated PL intensity spectra exhibiting a dramatic increase of PL signal with decreasing temperature. The numbers in brackets depict the scaling factor for the respective PL spectrum. For the two crystalline morphologies, the first spectra (298 and 200 K for bulk; 298, 200, and 150 K for microcrystal) were multiplied by a factor of 6 and 2, respectively. (b) Changes of the PL spectra normalized to the values at 298 K as a function of temperature. Both crystalline samples exhibit a PL increase upon reducing the temperature and saturation at low temperatures. Contrary, the PL signal of the amorphous film, after initial increase, is reduced for temperatures below 150 K.

TABLE I. (Color online) Characteristic decay parameters including standard deviations determined from the analysis of the temperature dependence of the steady state and transient PL spectra. The values refer to the energetic barriers and the lifetimes (inverse rates) as well as to the associated decay mechanisms for the different rubrene samples studied in this work. Lifetimes in bold correspond to the dominant decay channel at room temperature.

Sample type	$1/\gamma_{\mathrm{r}}$	$1/\gamma_{\mathrm{nr}}^{(1)}$	ΔE_1 (meV)	$1/\gamma_{\mathrm{nr}}^{(2)}$	ΔE_2 (meV)	$1/\gamma_{\mathrm{nr}}^{(3)}$	ΔE_3 (meV)
Bulk	Few ns	**(20 ± 4) ps**	44 ± 7	(100 ± 15) ps	25 ± 3	(500 ± 40) ps	134 ± 40
Micro	Few ns	–		**(100 ± 15) ps**	25 ± 3	(500 ± 40) ps	134 ± 40
Amorphous	Few ns	–		–		**(500 ± 40) ps**	134 ± 40

with activation energies observed for other long-range ordered molecular systems such as α-PTCDA single crystals [30].

By complementary time-resolved analysis of the PL spectra we are able to identify these fundamental decay channels and their dynamics dominating the transient excitonic behavior and, as demonstrated below, being in tight correlation with the respective degree of spatial confinement. The PL transients can be fitted by a standard, multiexponential behavior, e.g., comprising three nonradiative decay paths in the case of rubrene bulk crystals [Fig. 3(a)]. In accordance with Eq. (1) each channel is characterized by a specific decay time and correlated activation energy [29]

$$\tau^{-1} = \gamma = \gamma_{\mathrm{r}} + \gamma_{\mathrm{nr}}^{(1)} e^{-\Delta E_1/kT} + \gamma_{\mathrm{nr}}^{(2)} e^{-\Delta E_2/kT}$$
$$+ \gamma_{\mathrm{nr}}^{(3)} e^{-\Delta E_3/kT}. \quad (2)$$

At this point it is important to note that because of the linear relation between PL intensity and laser excitation power [see Fig. 3(c)] and the applied time window we can exclude bimolecular processes as well as delayed fluorescence by triplet fusion as additional decay channels [8].

At room temperature the PL decay of the bulk crystal is dominated by a nonradiative decay channel with a time constant of 20 ps ($1/\gamma_{\mathrm{nr}}^{(1)}$), which is consistent with the picosecond component found by Stöhr *et al.* [Fig. 3(d)] [13]. A second exponential component with an effective time constant of 100 ps is present ($1/\gamma_{\mathrm{nr}}^{(2)}$), however, yielding a much smaller contribution to the PL decay. The 20 ps relaxation channel is in excellent agreement with the reported rise time of the triplet absorption band due to singlet fission in rubrene single crystals and the estimated energetic barrier of 44 meV matches the offset between the energy of the excited singlet state S_1 and the summed-up triplet energy of $T_1 + T_1$ [22,24]. An additional ~2 ps component reported by Ma *et al.* could not be resolved in our measurements, presumably due to limitations by our setup.

As a key result of our investigation, in microcrystals this fission process cannot be identified. There the PL decay is rather governed by the 100 ps decay component with a corresponding activation energy of 25 meV deduced by the temperature dependence of the integrated PL spectrum. This observation can be directly correlated with the spatial confinement of optical excitations in the microcrystal volume and points towards a quenching mechanism appearing either on the outer surface or inner boundaries and leading to an

effective decay rate $\gamma_{\mathrm{nr}}^{(2)}$. An effective time constant of about 100 ps at room temperature has been also reported by Tao *et al.* [31] and was explained by formation of a polaronic absorption band upon exciton-polaron conversion. While the elementary dissociation mechanism could not be identified yet the results suggest a material-inherent channel which is in agreement with the assignment of a surface related process. Another possible loss scenario originates by the relaxation of singlet excitons into excitonic dark states at the interface. Theoretically, such a process related to next-neighbor molecular reorientation and accompanied by a conical intersection of the participating state manifolds has been predicted and was demonstrated to explain successfully the exciton diffusion properties of various polyaromatic hydrocarbons [28]. The local character of this decay channel is supported by the absence of lattice vibrational modes in this energy range [32]. As relaxation via triplet formation requires at least twice the activation energy of the 100 ps decay channel and as this energy is expected to be further enhanced by the reduced polarizability at the microcrystal boundaries, singlet fission is effectively suppressed in the microcrystals. This microscopic picture is supported by the observed elongation of the effective exciton lifetime by a factor of 5. Analyzing the PL decay dynamics in bulk rubrene crystals Wen *et al.* reported a 6.2 ps component attributed to singlet fission as well as a second time constant of 47 ps [33]. Whereas the fast channel cannot be detected due to the temporal resolution of our experimental setup, the time constant of the slower channel is significantly enhanced compared to the picosecond fission channel observed for bulk crystals in this work. This increase together with the associated activation barrier of 30 meV determined by Wen *et al.* point towards a stronger contribution by, e.g., interface quenching and illustrates the impact of morphological details at micrometer length scales on the exciton dynamics.

The third decay channel with a time constant of around 0.5 ns ($1/\gamma_{\mathrm{nr}}^{(3)}$) observed at room temperature, though much less pronounced, is in range of the effective radiative lifetime of the singlet excitons (intrinsic radiative lifetime: 16.5 ns [34]) and according to its energy results either from self-trapping by lattice relaxation or from inhomogeneities within the organic crystal acting as quenching sites during exciton migration. The influence of this channel is negligible for the photophysics of bulk single crystals but becomes relevant for exciton motion in the microcrystals presumably due to the mentioned increase
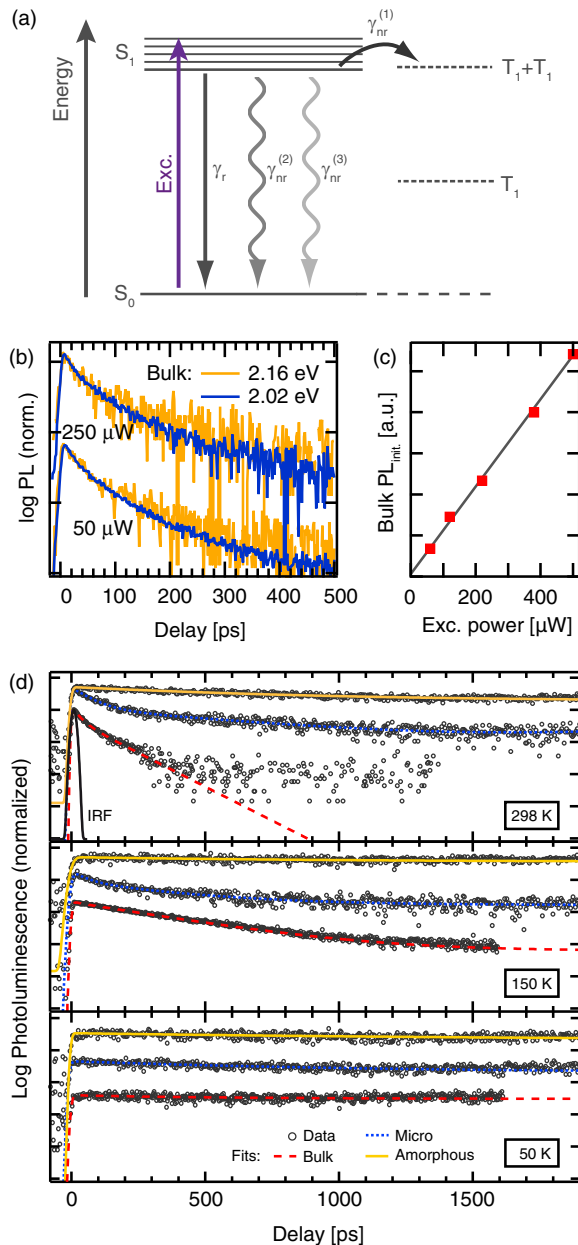
FIG. 3. (Color online) (a) Energy level scheme showing the possible relaxation pathways for singlet excitons in rubrene bulk crystals. (b) Bulk transients taken at 2.16 and 2.02 eV for two different excitation powers exhibit comparable decay dynamics indicating the presence of just one emitting excitonic species. (c) The initial PL peak height of the bulk morphology scales linearly with excitation power excluding bimolecular recombination processes as well as delayed luminescence. (d) Fits of the transient PL data taken at 2.16 eV for all three morphologies at room temperature, 150, and 50 K. The temperature dependent decay evidences the presence of thermally activated nonradiative decay channels.

of structural inhomogeneities as a result of the fast growth kinetics.

Due to the localized character of optical excitations, the decay of the PL signal for the amorphous film can be satisfactorily described by assuming solely the aforementioned long-lived nonradiative state of decay rate $\gamma_{nr}^{(3)}$. Interestingly,

as soon as the accessibility of interfaces is facilitated to an amorphous film of comparable thickness and surface flatness, e.g., by boundaries or dislocations, the decay dynamics change and become accelerated by a new dominating rate coinciding with $\gamma_{nr}^{(2)}$ (Fig. 7 in the Supplemental Material [17]). This observation can be explained by the effective increase of singlet excitons reaching these trapping sites and thus being quenched prior to alternative processes such as singlet fission. An additional decay time of about 2.2 ns has been reported by Piland *et al.* [35] for the spectrally integrated PL transients in amorphous rubrene films. However, this component which was assigned to singlet fission cannot be detected in our measurements presumably due to the time window of at most 2 ns in the utilized experimental setup. The fact that this time constant for singlet fission is larger by two orders of magnitude compared to studies by Ma *et al.* [24] as well as by us highlights the influence of structural disorder on the decay dynamics in amorphous rubrene.

Reducing the temperature of bulk and microcrystal leads to an increase of the average radiative lifetimes of the excitonic states as the decay via thermally activated nonradiative channels is incrementally hampered. Between 170 and 120 K the picosecond decay channels completely freeze out for bulk and microcrystal samples as the population density of phonons is strongly diminished. Therefore, despite its higher activation energy the $\gamma_{nr}^{(3)}$ channel remains the only nonradiative relaxation pathway for excitons at lower temperatures which cannot be explained by the mere anisotropy of the optical behavior.

The decay dynamics in this temperature regime are comparable to those of the amorphous sample: With decreasing temperature, i.e., decreasing exciton diffusion, the probability of reaching those quenching sites is reduced resulting in the observed increase of the average excitonic lifetimes. These lifetimes are of the order of a few nanoseconds in agreement with literature [8,13,18], but due to our experimental resolution can only be determined within a time frame of 2 ns. Nevertheless, from the transient data it can be concluded that due to the enhanced influence of interfaces the observed exciton lifetime for the microcrystals at low temperatures is slightly smaller compared to the two other morphologies.

In summary, we have demonstrated that the inherent length scales affect the excitation dynamics in rubrene samples of different morphology. We can ascribe their temperature and time-dependent PL behavior to the presence of three fundamental decay mechanisms, namely singlet fission, nonradiative relaxation by interface states and impurity quenching, and their respective predominance in the various morphologies. For single crystals we conclude that the spatial confinement on micrometer dimensions, which is typical for organic thin film devices, already has a massive influence on the temporal evolution of the PL. While the nonradiative decay in the rubrene single crystals is dominated by thermally activated singlet fission at a time constant of 20 ps and an activation barrier of 44 meV, this channel is effectively suppressed in microcrystal structures due to the presence of an additional decay mechanism related to the boundaries and characterized by an activation barrier of only 25 meV. As an important consequence, excitons reaching the grain boundaries of the microcrystals are trapped by surfaces states and transferred

to dark states or dissociated into polarons within 100 ps. A third relaxation channel of about 500 ps time constant becomes relevant for long range ordered rubrene stacks at very low temperatures. The local character of this decay path is indicated by its coincidence in time and energy with the only relaxation process observed for amorphous rubrene thin films and is attributed to interactions with impurities or self-trapping by lattice relaxation. Our findings clearly elucidate the effects by the local environment on the excitonic state dynamics of organic semiconductors. With respect to molecular thin film electronics, this correlation and the effects

emerging by confinement have to be considered in the ongoing miniaturization and in the development of innovative device concepts, such as photovoltaic cells based on triplet harvesting.

[1] P. Peumans, A. Yakimov, and S. R. Forrest, J. Appl. Phys. **93**, 3693 (2003).

[2] A. Rao, M. W. B. Wilson, J. M. Hodgkiss, S. Albert-Seifried, H. Bässler, and R. H. Friend, J. Am. Chem. Soc. **132**, 12698 (2010).

[3] P. J. Jadhav, P. R. Brown, N. Thompson, B. Wunsch, A. Mohanty, S. R. Yost, E. Hontz, T. V. Voorhis, M. G. Bawendi, V. Bulović, and M. A. Baldo, Adv. Mater. **24**, 6169 (2012).

[4] G. D. Scholes and G. Rumbles, Nat. Mater. **5**, 683 (2006).

[5] V. K. Thorsmølle, R. D. Averitt, J. Demsar, D. L. Smith, S. Tretiak, R. L. Martin, X. Chi, B. K. Crone, A. P. Ramirez, and A. J. Taylor, Phys. Rev. Lett. **102**, 017401 (2009).

[6] H. Najafov, B. Lee, Q. Zhou, L. C. Feldman, and V. Podzorov, Nat. Mater. **9**, 938 (2010).

[7] P. Irkhin and I. Biaggio, Phys. Rev. Lett. **107**, 017402 (2011).

[8] A. Ryasnyanskiy and I. Biaggio, Phys. Rev. B **84**, 193203 (2011).

[9] B. Verreet, P. Heremans, A. Stesmans, and B. P. Rand, Adv. Mater. **25**, 5504 (2013).

[10] S. Kowarik, A. Gerlach, S. Sellner, F. Schreiber, J. Pflaum, L. Cavalcanti, and O. Knovalov, Phys. Chem. Chem. Phys. **8**, 1834 (2006).

[11] D. Käfer and G. Witte, Phys. Chem. Chem. Phys. **7**, 2850 (2005).

[12] R. W. I. de Boer, M. E. Gershenson, A. F. Morpurgo, and V. Podzorov, Phys. Status Solidi A **201**, 1302 (2004).

[13] R. J. Stöhr, G. J. Beirne, P. Michler, R. Scholz, J. Wrachtrup, and J. Pflaum, Appl. Phys. Lett. **96**, 231902 (2010).

[14] P. Irkhin, A. Ryasnyanskiy, M. Koehler, and I. Biaggio, Phys. Rev. B **86**, 085143 (2012).

[15] R. A. Laudise, C. Kloc, P. G. Simpkins, and T. Siegrist, J. Cryst. Growth **187**, 449 (1998).

[16] D. H. Park, S. G. Jo, Y. K. Hong, C. Cui, H. Lee, D. J. Ahn, J. Kim, and J. Joo, J. Mater. Chem. **21**, 8002 (2011).

[17] See Supplemental Material at http://link.aps.org/supplemental/10.1103/PhysRevB.90.205305 for further information on the sample structure, integrated PL data and the effect of interfaces on the PL in case of amorphous films.

[18] H. Najafov, I. Biaggio, V. Podzorov, M. F. Calhoun, and M. E. Gershenson, Phys. Rev. Lett. **96**, 056604 (2006).

[19] N. Sai, M. L. Tiago, J. R. Chelikowsky, and F. A. Reboredo, Phys. Rev. B **77**, 161306 (2008).

[20] Y. Chen, B. Lee, D. Fu, and V. Podzorov, Adv. Mater. **23**, 5370 (2011).

[21] T. Petrenko, O. Krylova, F. Neese, and M. Sokolowski, New J. Phys. **11**, 015001 (2009).

[22] L. Ma, K. Zhang, C. Kloc, H. Sun, C. Soci, M. E. Michel-Beyerle, and G. G. Gurzadyan, Phys. Rev. B **87**, 201203(R) (2013).

[23] M. Nothaft and J. Pflaum, Phys. Status Solidi B **245**, 788 (2008).

[24] L. Ma, K. Zhang, C. Kloc, H. Sun, M. E. Michel-Beyerle, and G. G. Gurzadyan, Phys. Chem. Chem. Phys. **14**, 8307 (2012).

[25] A. Yildiz, P. T. Kissinger, and C. N. Reilley, J. Chem. Phys. **49**, 1403 (1968).

[26] T. S. Rose, R. Righini, and M. Fayer, Chem. Phys. Lett. **106**, 13 (1984).

[27] A. K. Topczak, T. Roller, B. Engels, W. Brütting, and J. Pflaum, Phys. Rev. B **89**, 201203(R) (2014).

[28] V. Settels, A. Schubert, M. Tafipolsky, L. Wenlan, V. Stehr, A. K. Topczak, J. Pflaum, C. Deibel, R. Fink, V. Engel, and B. Engels, J. Am. Chem. Soc. **136**, 9327 (2014).

[29] N. J. Turro, V. Ramamurthy, and J. Scaiano, *Modern Molecular Photochemistry of Organic Molecules* (University Science Books, Sausalito, CA, 2010).

[30] A. Y. Kobitski, R. Scholz, D. R. T. Zahn, and H. P. Wagner, Phys. Rev. B **68**, 155201 (2003).

[31] S. Tao, H. Matsuzaki, H. Uemura, H. Yada, T. Uemura, J. Takeya, T. Hasegawa, and H. Okamoto, Phys. Rev. B **83**, 075204 (2011).

[32] E. Venuti, I. Bilotti, R. Della Valle, A. Brillante, P. Ranzieri, M. Masino, and A. Girlando, J. Phys. Chem. C **112**, 17416 (2008).

[33] X. Wen, P. Yu, C.-T. Yuan, X. Ma, and J. Tang, J. Phys. Chem. C **117**, 17741 (2013).

[34] S. L. Murov, I. Carmichael, and G. L. Hug, *Handbook of Photochemistry*, 2nd ed. (Marcel Dekker, New York, 1993).

[35] G. B. Piland, J. J. Burdett, D. Kurunthu, and C. J. Bardeen, J. Phys. Chem. C **117**, 1224 (2013).